

H. Dothe, J.W. Duff, J.H. Gruninger, R. Panfili, R. Kennett, J.H. Brown, Auroral radiance modeling with SAMM@2, Proc. SPIE 7475, Remotes Sensing of Clouds and the Atmosphere XIV, 834043 (2009).

Copyright 2009 Society of Photo-Optical Instrumentation Engineers. One print or electronic copy may be made for personal use only. Systematic reproduction and distribution, duplication of any material in this paper for a fee or for commercial purposes, or modification of the content of the paper are prohibited.

<http://dx.doi.org/10.1117/12.834043>

See next page.

Auroral radiance modeling with SAMM2

H. Dothe^{*a}, J. W. Duff^a, J. H. Gruninger^a, R. Panfili^a, R. Kennett^a, J. H. Brown^b

^aSpectral Sciences, Inc., 4 Fourth Avenue, Burlington, MA USA 01803-3304

^bAir Force Research Laboratory/RVBYB, 29 Randolph Road, Hanscom AFB, MA USA 01731

ABSTRACT

This paper presents results that demonstrate the auroral modeling capabilities of the Air Force Research Laboratory (AFRL) SAMM2 (SHARC And MODTRAN[®] Merged 2) radiance code. A scene generation capability is obtained by coupling SAMM2 with a recently developed Clutter Region Atmosphere and Scene Module (CRASMO), which provides an approach for rapid generation of time sequences and images of radiance clutter. Modeled results will be compared to data collected by the Midcourse Space Experiment (MSX)¹ in the IR and UV-visible spectral regions during an auroral event on November 10, 1996.

The paper is organized as follows. We first present a brief history of the AFRL SHARC/SAMM codes, leading up to the current version, SAMM2 v.2. The SAMM2 UV-visible auroral kinetic model will then be described, followed by a comparison of modeled results to the MSX data.

Keywords: Aurora, UV-Visible, IR, radiance scene

1. BRIEF OVERVIEW OF THE SHARC/SAMM RADIANCE CODES

The current SAMM2 code base² represents nearly two decades of active development of an atmospheric background capability. Development began in 1989 with the introduction of SHARC, the Strategic High-Altitude Radiance code.³ The initial goal of this code was to provide a first-principles model of the high-altitude non-LTE (non Local Thermodynamic Equilibrium) environment. SHARC considered the vibrational states of atmospheric radiators as non-LTE and allowed user-adjustable chemical kinetics mechanisms and rate constants. The original SHARC code considered seven radiators: three isotopes of CO₂, four isotopes of H₂O, O₃, NO, OH and CH₄. The code operated in the infrared with a spectral range of 2-40 μm with a maximum output spectral resolution of 1 wavenumber. Interaction with the code was available through text-driven user interface. Arbitrary lines of sights (LOSs) traversing altitudes no lower than 40 km above the ground were supported.

Over time, the capabilities of SHARC were expanded to incorporate a number of new phenomenologies. The 1991 release of SHARC-2 introduced a radiance modeling capability for auroral conditions. To support this new feature, important generators of infrared auroral radiance were introduced, including CO₂(v₃), NO and NO⁺. Rate constants for important reactions in auroras were obtained from the AFRL AARC (Auroral Atmospheric Radiance Code) program.⁴ A multiple region capability was implemented to allow for the definition of the local, aurorally enhanced region with its own atmospheric chemistry. SHARC-2 supports LOSs traversing arbitrary paths through the ambient and auroral regions at altitudes no lower than 40 km above the ground. The 1993 release of SHARC-3 introduced a twilight modeling capability, i.e., solar terminator condition. This was accomplished by introducing the concept of multiple atmospheric profiles into the code. Each profile can contain a unique solar zenith angle, allowing a smooth transition from day to night. Along with this addition was the creation of an off-line tool capable of generating consistent atmospheric profiles: the user-defined SHARC Atmospheric profile Generator (SAG) which accounts for temporal, geographical and geophysical variabilities. The 1997 release of SHARC-4⁵ added an atmospheric stochastic structure capability to model radiance clutter. With it, estimates of the radiance fluctuations associated with temperature variations in the atmosphere were obtained.

*dothe@spectral.com; phone 781 273-4770; fax 781 270-1161; www.spectral.com

SHARC, however, remains limited as a high-altitude code only. The SAMM code (SHARC and MODTRAN[®] Merged) was introduced to circumvent this limitation. It integrated MODTRAN^{®6}, a standard low-altitude LTE code, with SHARC to produce a single code. SAMM maintains the flexibility of SHARC while introducing the low-altitude capabilities of MODTRAN[®]. This new code had a moderate spectral resolution of 1 cm⁻¹. Like SHARC, it was an infrared code with a spectral range that was extended down to 1 micron. SAMM is able to support an arbitrary LOS from the ground to the edge of the atmosphere while maintaining all of the previously created capabilities within SHARC. In addition, the SAG atmospheric generator was updated to provide atmospheric properties for the full altitude range supported in SAMM as well as the ability to generate MODTRAN[®]-specific atmospheres for MODTRAN[®] calculations.

The next major revision to the code base was released in 2003. SAMM2 was a rewrite of the SAMM code base into a single, *seamless capability with a unified RT algorithm*. It maintained the essential low-altitude databases of the MODTRAN[®] code (clouds, aerosols, and surface reflectance) as well as the DISORT multiple scattering capability and MODTRAN[®] refractive geometry code. All of the key features of SHARC-4 were maintained, including non-LTE chemical kinetics, auroral modeling, solar terminator modeling, and stochastic structure computations. SAMM2 introduced a next-generation full-featured line-by-line code coupled with a novel treatment of line tails. As a result, SAMM2 combines the key capabilities of MODTRAN[®], FASCODE, and SHARC and is capable of producing background scenes consisting of a large number of unique LOSs. At this time, a new SAG2 climatology model was introduced which supported the NLR MSISE 2000 model along with additional water databases.

The next major revision to the code base is scheduled to be completed in 2010. The spectral range of all the SHARC/SAMM codes up to this point has been the IR. For the next revision, comprehensive coverage from the infrared through ultraviolet 0.3 to 40 μm (250 to 33,000 cm⁻¹) wavelength region will be provided for arbitrary LOSs in the 0-300 km altitude regime. The new code has also optimized the usage of computational resources, resulting in a substantial reduction in memory usage and a ten-fold increase in the computational speed of the line-by-line algorithm. Additionally, more approximate non-LTE correlated-*k* and band models have also been introduced to provide speedy computations in applications where the utmost accuracy is not required.

It is the extension of the code spectral range into the UV-Visible region that will be the focus of this paper. In the next section, we briefly describe the SAMM2 UV-visible model.

2. SAMM2 UV-VISIBLE MODEL

A UV-Visible model was implemented in SAMM2 v.2, the most recent version of the SAMM2 code, extending the spectral range down to 0.3 μm. The kinetics for existing SAMM2 v.2 IR species emitting in the visible spectral region have been augmented to support the new visible/ultraviolet capability. Existing SAMM2 v.2 IR species (vibrationally excited) emitting in the visible spectral region already include LTE vibrationally excited radiators, such as SO₂ and NO₂, as well as the NLTE vibrationally excited radiators, O₃, CO₂, H₂O and OH. Highly vibrationally excited states of water emitting in the visible are formed by H₂O + O, O₂, N₂. Additionally, highly excited states of OH (v=6 - 9) can be formed by H + O₃ reactions, leading to the OH Meinel bands.

A more complete extension into UV-visible region requires incorporation of NLTE electronically excited states of O₂, N₂ molecules and their ions, as well as electronically excited states of O, N, O⁺, and N⁺. The current version includes electronically excited species and emission bands consistent with AURIC (Atmospheric Ultraviolet Radiance Integrated Code)⁷, i.e., the N₂ electronic transition bands (VK, 1PG, 2PG), N₂⁺ (Meinel and 1NG) bands, O₂ (ATM, Herzberg) bands, as well as the O, O⁺ and N atomic lines.

The excitation into high electronic levels is triggered by solar radiation in the daytime, and by primary electron bombardment in auroras. The different processes producing electronically excited species, denoted by asterisks, are summarized as follows,

- Daytime chemistry is driven by
 - Photodissociation: $h\nu + \text{O}_2, \text{N}_2 \rightarrow \text{O} + \text{O}^*, \text{N} + \text{N}^*$
 - Photoionization: $h\nu + (\text{O}_2, \text{N}_2, \text{O}) \rightarrow (\text{O}_2^{+*}, \text{N}_2^{+*}, \text{O}^{+*}) + e$
 - Photodissociative ionization:
 - $h\nu + (\text{O}_2, \text{N}_2) \rightarrow (\text{O}^{+*} + \text{O}, \text{N}^* + \text{N}^+) + e$
 - Electron Impact Excitation: $(\text{O}, \text{N}_2) + e \rightarrow (\text{O}^*, \text{N}_2^*) + e$
 - Electron Impact Dissociation: $\text{N}_2 + e \rightarrow \text{N}^* + \text{N}^{**} + e$

- Electron Impact Ionization:
 - $(O_2, N_2, O) + e \rightarrow (O_2^+, N_2^+, O^+) + e + e'$
- Electron Impact Dissociative Ionization:
 - $(O_2, N_2) + e \rightarrow (O + O^+, N^+ + N^+) + e + e'$
- Under auroral conditions, energy deposition by primary electrons e_p replaces the solar flux $h\nu$ in the three photo-driven processes shown above. Ionization and dissociative ionization produce secondary electrons, which trigger ensuing e-impact processes.
- Resulting excited and ionic species from above production trigger chemical reactions leading to electronically excited species that emit UV-visible radiance.
- Nighttime quiescent radiance, predominantly from oxygen, is driven by O/O₂ chemistry:
 - $O^+ + e \rightarrow O^*$
 - $O^+ + O_2 \rightarrow O + O_2^+$
 - $O_2^+ + e \rightarrow O + O^*$
 - $O + O + M \rightarrow O_2^* + M$

An example of SAMM2 spectral radiances in the daytime visible spectral range is shown in Fig. 1.

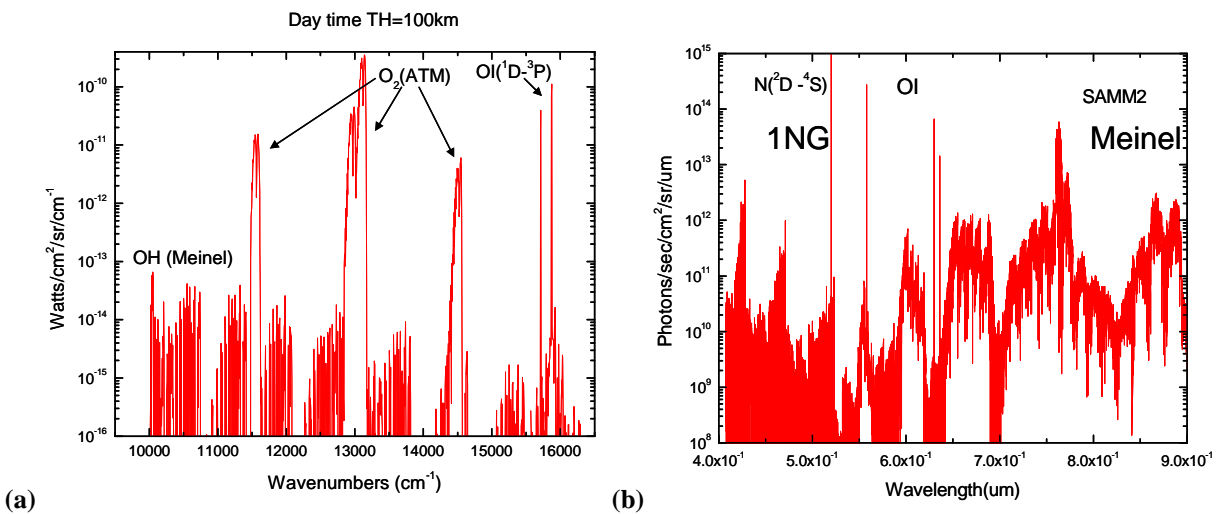


Fig. 1. SAMM2 calculated daytime TH=100km limb spectral radiances of (a) OH Meinel Band, O₂ ATM band, (b) N₂⁺ 1NG and Meinel bands. OI and NI atomic emissions are shown.

In the next section, an application of SAMM2 to model IR and UV-visible radiances observed during an aurora by the MSX experiments will be described.

3. SAMM2 MODELING OF MSX AURORAL DATA

3.1 Previous work

The auroral event observed by the MSX satellite on November 10, 1996 has previously been modeled by several of this paper's authors Sharma *et al.*⁸, as well as by Strickland *et al.*⁹ Using a value of ~ 8 KeV for the primary electrons average characteristic energy determined by the Strickland group, we derived an aurorally dosed region that allowed us to reproduce the Band A (6μm-11μm) radiances measured by the SPIRIT III Radiometer instrument aboard the MSX satellite.⁸ The Band A radiance was shown to arise from emission due to vibrationally and rotationally excited NO formed during the aurora. In this paper, we have used the same auroral region to model the N₂⁺ 1NG (391.4 nm) emission measured by the MSX SPIM, using the SAMM2 UV-visible auroral model described in section 2. For reference, we show some of our previous results from Sharma.⁸ The auroral region is reproduced below in Fig. 2, and the 5.3μm NO spectra computed by the SHARC aurora model (now part of SAMM2) together with the Band A filter, as well as model results and MSX data, are reproduced in Fig. 3.

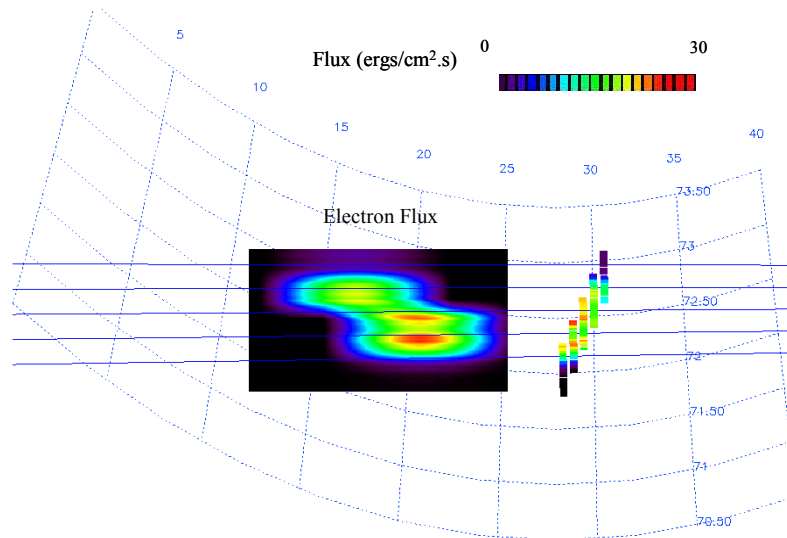


Fig. 2. Aurorally dosed region [Sharma et al., (2001)]. Fluxes are shown on a latitude/longitude grid, characteristic energy $E_0=8\text{KeV}$.

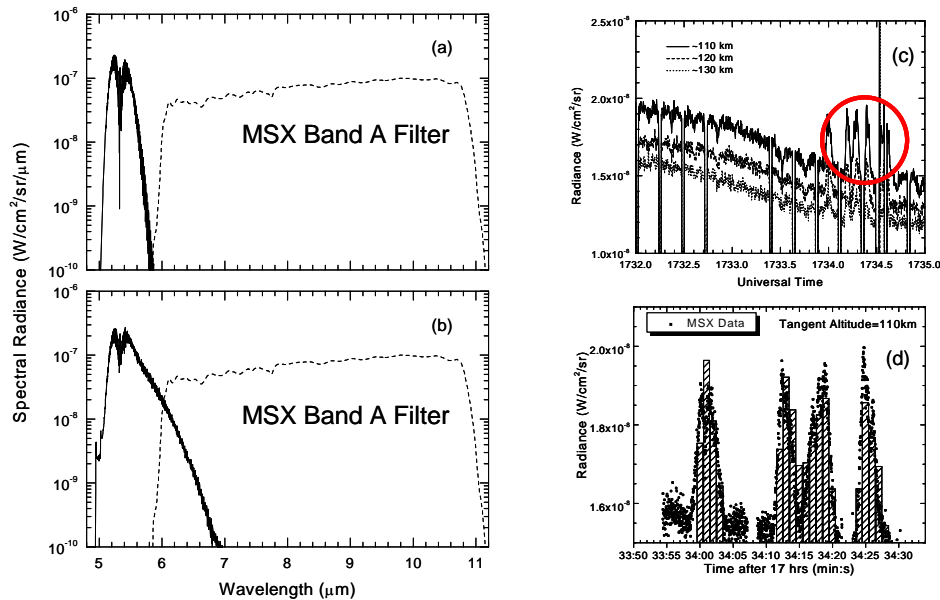


Fig. 3. Aurorally enhanced NO (a) Emission from rotationally thermal NO($v=1$) from O+NO (b) Emissions from vibrationally and rotationally hot NO from $\text{N}^4\text{S}, ^2\text{D} + \text{O}_2$. (c) SPIRIT III Band A data (d) SHARC aurora model results vs. SPIRIT III data. From Sharma, et al.⁸

In the next subsection, we briefly describe a recently developed toolkit that, coupled with SAMM2 results, allows for the creation of radiance scenes that can be compared to the MSX SPIM data.

3.2 SAMM2 scene generation capability

To generate radiance scenes from SAMM2 results, we have utilized a recently developed toolkit for SAMM2, dubbed CRASMO (Clutter Region Atmosphere and Scene Module). CRASMO defines the geophysical parameters for the modeled scene, generates the necessary profiles for the multiple atmospheric regions including the auroral region, incorporates the sensor viewing angles to generate the multiple LOSs for SAMM2 runs and post-processes the outputs to compute the scene radiances. Examples of SAMM2/CRASMO scenes are shown in Fig. 4. Figure 4 illustrates the effect of the primary electron energy on the auroral radiance limb profile in the MSX B2 Band ($\sim 2361 \text{ cm}^{-1}$). The larger characteristic energy caused a deeper penetration and a stronger emission from a lower tangent height.

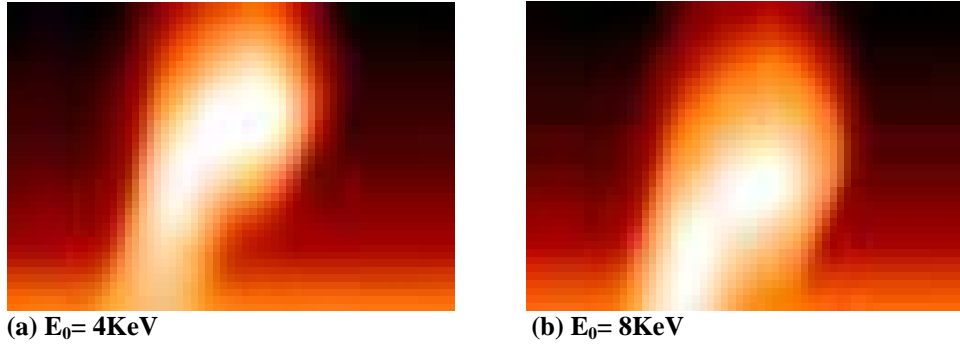


Fig. 4. Effect of the primary electron energy on the auroral radiance limb profile in the MSX B2 Band ($\sim 2361 \text{ cm}^{-1}$). Altitudes of Emissions in the B bands are very sensitive to the Characteristic Energy of the electrons.

3.3 Results from SAMM2 UV-Visible aurora model

Calculated results generated by SAMM2 using input files from the CRASMO scene toolkit are shown in Fig. 5. Comparisons with two selected SPIM scenes show good agreement between model and data.

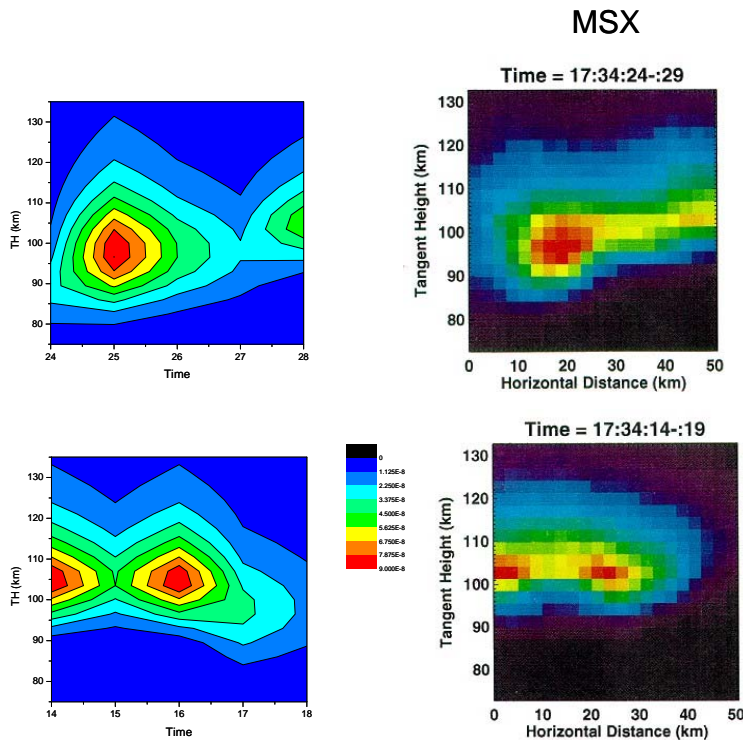


Fig. 5. Comparisons between SAMM2 results and MSX SPIM scenes in the 391.4nm region.

The occurrence of maximum radiance at lower tangent height $\sim 95\text{km}$ for time=17:34:24-:29 can be explained by the satellite moving closer to a strongly dosed region on the near side of the tangent point, i.e., the aurora moving further away from the tangent point, as shown for the top two LOSs illustrated in Fig. 2. These results are consistent with conclusions by Strickland, et al.⁹ and Sharma, et al.⁸

SAMM2 spectral radiances are compared to the MSX SPIM data⁹ in Figs. 6 and 7. Qualitative consistency is shown through the UV-visible spectral range from 140 nm to 580 nm. The N_2 (VK, 2PG, LBH) and N_2^+ (1NG) bands are well reproduced, as well as the O green line, while the SAMM2 model does not currently include Lyman (α, β), OI (130., 135, 297.), O^+ and N^+ emissions. Additionally, the auroral model does not currently include $\text{N}_2(\text{X}, \nu)$ states with $\nu > 5$, so the LBH sequence from 180nm to 240 nm is not modeled.

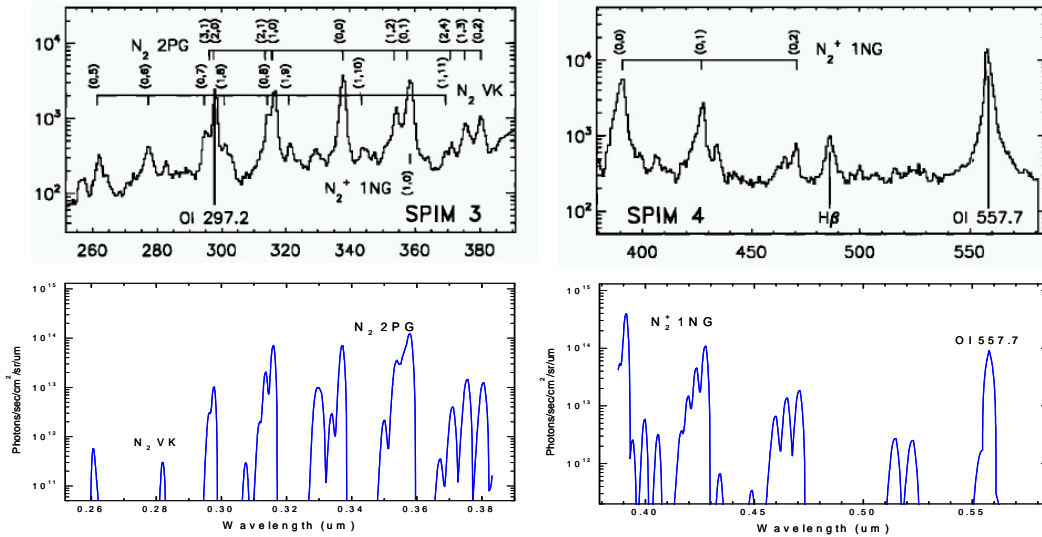


Fig. 6. Comparison between SAMM2 spectral radiances and MSX SPIM 3 and 4 (see text).

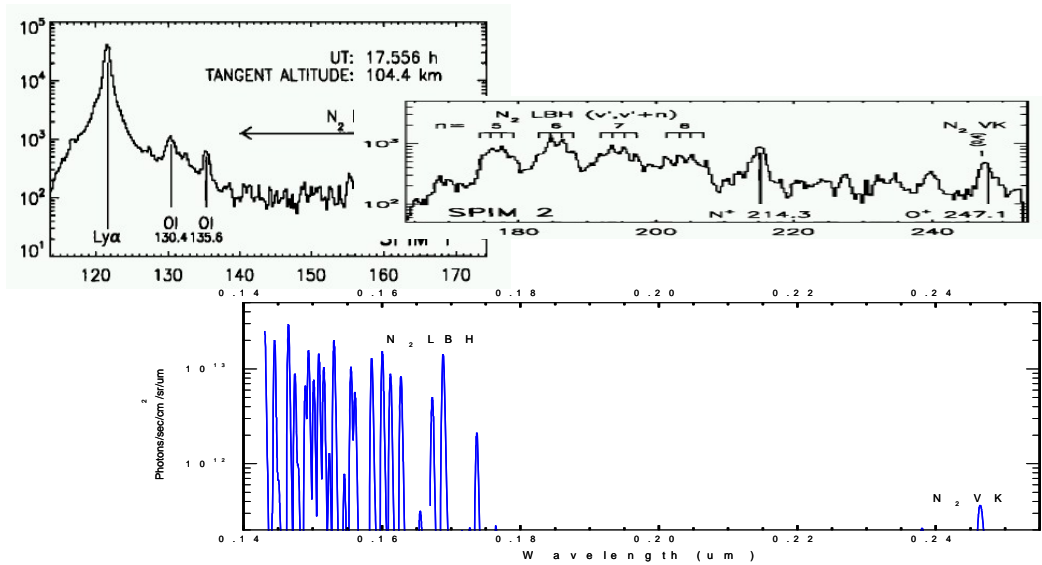


Fig. 7. Comparison between SAMM2 spectral radiances and MSX SPIM 1 and 2 (see text).

4. CONCLUSIONS

Ambient UV-Visible daytime and auroral chemistry models have recently been integrated into latest modern version of SAMM2, extending the spectral resolution to 0.3 um. Results from the SAMM2 auroral model were previously validated in the IR region against the MSX NO data (Band A).⁸ In this paper, SAMM2 aurora modeling and scene generation capabilities have been demonstrated in the UVISI spectral region. Scenes generated by the SAMM2 auroral model of N_2^+ 1NG emissions are found to be in good agreement with the MSX 391.4 nm SPIM data. Qualitative consistency have additionally been obtained against MSX N_2 (VK, 2PG, LBH) data.

The SAMM2 Aurora Kinetic Models continue to be fine tuned, including incorporating updated electron impact cross sections, ion chemistry reaction rates, and including a rotational NLTE model for NO radiance.

5. REFERENCES

- [1] Mill, J. D., Neil, R. O., Price, S., Romick, G. J., Uy, O. M., Gaposchkin, E. M., Light, G. C., Moore Jr., W. W. J and Murdock, T. L., "Midcourse Space Experiment: Introduction to the spacecraft, instruments and scientific objectives," *J. Spacecr. Rockets* 31, 900 (1994).
- [2] Dothe, H., Duff, J. W., Gruninger, J. H., Acharya, P. K., Berk, A., Brown, J. H. and Sharma, R. D., "Users' Manual for SAMM2, SHARC-4 and MODTRAN[®]4 Merged," Air Force Research Laboratory, AFRL-VS-HA-TR-2004-1145 (2004).
- [3] Sundberg, R.L., Duff, J.W., Gruninger, J.H., Bernstein, L.S., Matthew, M.W., Adler-Golden, S.M., Robertson, D.C., Sharma, R.D., Brown, J.H., and Healey, R.J., "SHARC, a Model for Calculating Atmospheric Infrared Radiation Under Non-Equilibrium Condition," *Geophysical Monograph Series*, 87, 287 (1995).
- [4] Winick, J. P., Picard, R. H., Joseph, R. A., Sharma, R. D. and Wintersteiner, P. P., "AARC: the Auroral Atmospheric Radiance Code," AFGL-TR-87-0334, ADA202432 (1987).
- [5] Duff, J. W., Gruninger, J. H., Brown, J. H., Sharma, R. D., Blumberg, W. A. M. and Grossband, N., "SHARC-4: A model for atmospheric background radiance structures," *Proc. 1996 Meeting of the IRIS Specialty Group on Targets, Backgrounds, and Discrimination* (1996).
- [6] Berk, A., Bernstein, L. S. and Robertson, D. C., "MODTRAN[®]: A moderate resolution model for LOWTRAN 7," GL-TR-89-0122, (1989).
- [7] Strickland, D. J., Bishop, J., Evans, J. S., Majeed, T., Shen, P. M., Cox, R. J., Link, R. and Huffman, R. E., "Atmospheric Ultraviolet Radiance Integrated Code (AURIC): theory, software architecture, inputs and selected results," *JQSRT* 62, 689-742 (1999).
- [8] Sharma, R. D., Neil, R. O., Gardiner, H., Gibson, J., Dothe, H., Duff, J. W., Wintersteiner, P. P. and Kendra, M., "Midcourse Space Experiment: Auroral enhancement of nitric oxide medium-wave infra red emission observed by the Spatial Infrared Imaging Telescope III radiometer," *JGR* 106, 21,351-21,365 (2001).
- [9] Strickland, D. J., Bishop, J., Evans, J. S., Majeed, T., Cox, R. J., Morrison, D., Romick, G. J., Carbary, J. F., Paxton, L. J. and Meng, C. I., "Midcourse Space Experiment/Ultraviolet and Visible Imaging and Spectrographic Imaging limb observations of combined proton/hydrogen/electron aurora," *JGR* 106, 65-75 (2001).